**Aalborg Universitet**

AALBORG UNIVERSITY
DENMARK

# Characterization and Modeling of the User Blockage for 5G Handset Antennas

Liu, Peiye; Syrytsin, Igor Aleksandrovich; Nielsen, Jesper Ødum; Pedersen, Gert Frølund; Zhang, Shuai

*Published in:*
I E E E Transactions on Instrumentation and Measurement

*DOI (link to publication from Publisher):*
10.1109/TIM.2020.3039644

*Creative Commons License*
Unspecified

*Publication date:*
2021

*Document Version*
Accepted author manuscript, peer reviewed version

Link to publication from Aalborg University

*Citation for published version (APA):*
Liu, P., Syrytsin, I. A., Nielsen, J. Ø., Pedersen, G. F., & Zhang, S. (2021). Characterization and Modeling of the User Blockage for 5G Handset Antennas. *I E E E Transactions on Instrumentation and Measurement*, *70*, 1-11. [9265270]. https://doi.org/10.1109/TIM.2020.3039644

**General rights**
Copyright and moral rights for the publications made accessible in the public portal are retained by the authors and/or other copyright owners and it is a condition of accessing publications that users recognise and abide by the legal requirements associated with these rights.

- Users may download and print one copy of any publication from the public portal for the purpose of private study or research.
- You may not further distribute the material or use it for any profit-making activity or commercial gain
- You may freely distribute the URL identifying the publication in the public portal -

**Take down policy**
If you believe that this document breaches copyright please contact us at vbn@aub.aau.dk providing details, and we will remove access to the work immediately and investigate your claim.

Downloaded from vbn.aau.dk on: May 04, 2023

# Characterization and Modeling of the User Blockage for 5G Handset Antennas

Peiye Liu, Igor Syrytsin, Shuai Zhang, *Senior Member IEEE*, Jesper Ødum Nielsen, Gert Frølund Pedersen, *Senior Member IEEE*

***Abstract*—In this work a stochastic 3D user shadow model is presented which can be used in the frequency range from 28 GHz to 34 GHz. To characterize the user shadowed pattern new metrics of shadowed cumulative distribution function (SCDF) and user shadowed intensity ratio (USIR) are proposed. The user shadow model is based on measurements with 18 subjects of different heights and gender. For simplicity the user shadow pattern is divided into four regions based on the mean shadow pattern obtained from the measurements. Each of the spatial regions is modeled as a stochastic process which follows the Gaussian distribution. It has been shown that any horizontally polarized mobile antenna is compatible with the presented model. The proposed user shadow pattern model can be directly used for the 5G mm-wave ray tracing or link simulations.**

***Index Terms*—Mobile terminal antenna, antenna array, 5G, mm-wave, shadowing, user impact, blockage.**

## I. Introduction

In the recent few years 5th generation (5G) wireless communication systems have attraced a high level of interest and been developed rapidly. One of the main purposes of 5G is to provide users with high throughput. This goal can be achieved in multiple different ways, for example increasing the number of transmit and receive antennas or increasing the bandwidth of the system. For the 5G massive MIMO systems, besides the frequencies below 3.5 GHz, microwave and millimeter wave frequencies will also be occupied in order to obtain wider bandwidth [1]. In 2017, multiple candidate bands between 24.25 GHz and 86 GHz have been proposed at the World Radiocommunication Conference [2]. However, at the microwave and millimeter wave frequencies the path loss becomes more severe, but transmitting with more power is not a viable solution as it will create more interference to the co-channel cells and also will drain the battery of the mobile terminal more quickly. One of the solutions to this problem is to increase the gain of the antennas [3]. Base stations are already equipped with multiple high gain antennas, but at mobile terminal side, a high gain antenna are more challenging to implement because of the device size limitations. Furthermore, a spatial beamforming technique will be required in order to steer the main beam of the antenna towards the base station. A full spatial coverage is also required from the handset antenna which can be oriented in any possible way. Spatial coverage can be characterized by using a coverage efficiency metric, which has been proposed in [4] and then used to assess the performance of the 5G handset antennas in [5].

However, to assess mobile comunication links, only saptial coverage of antenna is not enough. The handset antenna and the user cannot be so easily separated. Human body effect has been considered as a part of human body communications, a statistical investigation was conducted under 100MHz in [6]. And in [7], human body shadowing effect is accessed to reduce positioning error in ultrawideband ranging system. In [8], RF field strength is measured in human exposure evaluation up to 2.7GHz. Furthermore, human effect on total radiated power and 3-D radiation pattern is analysed at Global System for Mobile communications (GSM) 900/1800 in [9], up to 8 dB body loss is shown due to user's hand and head blockage. Study of whole body influence at 2.1 GHz reported in [10] and 0.5 −3GHz in [11] both showed significant efficiency decrease caused by user blockage. However, studies [6]–[11] are all at sub 6GHz bands, significant blockage from the user is expected at the mm-wave frequencies [12], although the body loss is much lower than that at sub 6GHz bands. At 15 GHz the user effects have been measured with a phased array in [13], and a strong shadowing effect from the human body of around 20-25dB is observed and significant losses in the coverage efficiency have been recorded. Blockage from the user is not as severe at 28 GHz as that at 60 GHz [14], but still should be considered when assessing the performance of the 5G mm-wave mobile communication link. The 3GPP community has already proposed some models for the user shadowing [15]. However, those models are highly inaccurate and extremely simplified. One of the modes represents the user blockage by a rectangular space with −30 dB attenuation inside. In real life the user's body shadow shape is more complicated than a rectangular space, and also in addition to the diffractions, creeping waves and surface waves will change the shape of the user blockage considerably. The user shadowing pattern can be affected by many aspects, such as main beam direction, antenna polarization and directivity, antenna position on the ground plane, user's grip and many more others. The effects of the phone case on the performance of the antennas has been investigated in [16] and significant changes in the shape of the radiation pattern have been observed. However, by adding the two-tilted layers of coupled metal strips, placed at the borders of the frame, the blockage by the metal frame is reduced significantly as shown in [17]. The investigation of user effects on the phased and switch diversity antenna arrays in [18] has shown that phased arrays have different performance due to antenna-user oritation. It has also been shown that user effects

This work was supported by the User Shadowing project with Huawei Gothenberg, Sweden.(Corresponding author: Shuai Zhang).

Peiye Liu, Igor Syrytsin, Shuai Zhang, Jesper Ødum Nielsen, and Gert Frølund Pedersen are with the Antennas, Propagation and Millimeter-wave Systems section at the Department of Electronic Systems, Aalborg University, Denmark (email: {igs,sz,gfp}@es.aau.dk).

can be mitigated by using antenna array diversity in [19]. Finally, in [20] the blockage from the user's hand and body is measured with the phased array in the indoor environment. However, in this case only the received power is measured and no spatial distribution has been given. The model proposed in that study only works for the specific handset-base station setup and can not be considered a general model, because user blockage also highly depends on the such parameters as handset antenna oritation, height, antenna-user distance and so on which are investigated in this paper to have a accuracy model of the user blockage for 5G terminals.

In this paper a user shadow model based on the measurements with the 18 users with the most critical gestures is presented. In Section II, the measurements are done in the anechoic chamber with the user applying different gestures in order to find out which handset positions have the biggest impact on the user blockage. A new metric of shadowed cumulative distribution function (SCDF) is proposed to characterize the variations inside the user shadow region. Then in Section III, it has been shown that the user shadowed intensity ratio (USIR) can be reliably extracted from the measurements with the user with help of the free space radiation pattern of the antenna under test (AUT). Furthermore, it has been found that the de-embedded user shadowed intensity ratio is not sensitive to the antenna beam width with the same polarization. Next in Section IV, the measurements with multiple user are conducted. In respect to measurement campaign in [12], 18 subjects have been chosen in consideration of the human height distribution. In this section, the mean radiation patterns and USIRs for both data and dual hand modes are presented. Finally in Section V, the stochastic model of USIR is proposed. The modeled mean USIR (Obtained from multiple random process realizations) is compared with the measured mean USIR and shows high similarities. The model is much more closer to the actual measured user shadowed patterns than the 3GPP models.

## II. Critical Gesture Investigation

In this section, multiple common user gestures are investigated. Multiple measurements are performed to find out which user gestures yield the highest blockage. Besides the radiation patterns, two other metrics will be used in the work to assess the user shadow. First, the shadowed antenna power ratio (SAPR) metric is applied to quantify the shadowed power. The amount of the power in the shadow region in comparison with the total power radiated by the antenna in the free space is called SAPR which is proposed in [12].

The SAPR is defined as:

$$\begin{aligned} &SAPR(\delta\theta,\delta\phi) \\ &= \frac{P_{shadow}}{P_{total}} \\ &= \frac{\Delta\phi\Delta\theta\sum_{\theta_{min}}^{\theta_{max}}\sum_{\phi_{min}}^{\phi_{max}}(P_{ant,V}(\theta,\phi)+P_{ant,H}(\theta,\phi))sin(\theta)}{\Delta\phi\Delta\theta\sum_{1^\circ}^{140^\circ}\sum_{-180^\circ}^{180^\circ}(P_{ant,V}(\theta,\phi)+P_{ant,H}(\theta,\phi))sin(\theta)} \end{aligned} \quad (1)$$

In the formula, $P_{shadow}$ describes the power in the shadow (in the chosen area of a radiation pattern) and integrated from the center of the shadow (at 0° ) towards both positive and negative axes in angle $\phi$ and from the start to the end point in angle $\theta$. $P_{total}$ is the TRP with the user. The lower the SAPR level is, the stronger the shadow loss is in the chosen spatial region.

Then, the shadowed cumulative distribution function (SCDF) is used to show how the power intensity within the user shadowed region is distributed.

The SCDF is defined as:

$$F(x) = P(X \leq x) \quad (2)$$

$P$ is the probability of the power of spatial piont $X$ in the shadowing region takes on a value less than or equal to a certain power level $x$.

### A. Measurement setup

In this paper, all the measurements are performed in the anechoic chamber at the Antennas, Propagation and Millimeter wave Systems laboratory at Aalborg University. The measurement setup is shown in Fig. 1. The styrofoam column with the adjustable height is used to fix the position of the antenna under test (AUT), while the user stands on the platform with its back against the wooden pole, holding the AUT. During the measurement, the platform turns in azimuth angle $\phi$, and then the probe on a robot arm scans in inclination angle $\theta$ with steps. The wooden pole is added for the user's safety, as in the measurement the platform is raised up to around 3.5 m height to ensure that the AUT is at the center of the measurement system. The system is able to measure in the maximum range of $-180^\circ$ to $180^\circ$ in $\phi$ angle, and $1^\circ$ to $140^\circ$ in $\theta$ angle. The bottom $40^\circ$ is not considered as the metal platform will totally block that area.

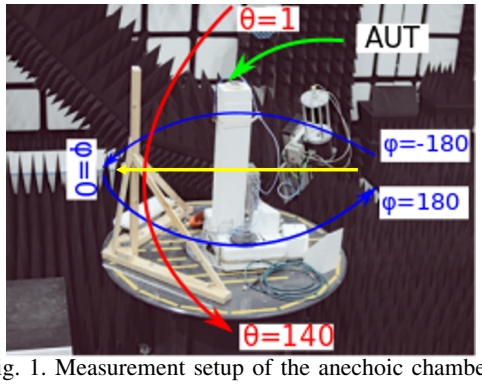

Fig. 1. Measurement setup of the anechoic chamber.

In the measurements a single wideband dipole antenna element located in the center of the array is used as the AUT. The chosen antenna operates from 28 GHz to 34 GHz [12]. Fig. 2(a) shows the free space radiation pattern under the measurement setup. A shadow seen at $\phi = 0^\circ$ is due to the blockage by the wooden pole. however during the measurement, the user is standing in between of the AUT and the wooden pole, which means that the wooden pole will be behind the user's back and is not visible from the viewpiont of the AUT in the measurement. Thus, most of the power will be absorbed and blocked by the user, or reflected back. Then with the same setup, AUT and user with the same standing way,

the effect of the wooden pole can be neglected in user shadow investigations. SAPRs at the four operating frequencies are shown in Fig. 2(b) with the user with the same gesture. To compare the antenna performance within the frequency range, the miss-match losses and radiation efficiency of the antenna are calibrated out. It can be seen that the SAPR difference is only around 1dB at 80° window size which includes the diffraction, creeping wave and surface wave. SAPR does not depend on frequency in the operation range of the AUT, which is why further measurements are only performed at a single frequency 28 GHz which is more attractive for 5G terminals instead of the whole operating bandwidth which will increase the measurement time considerably.

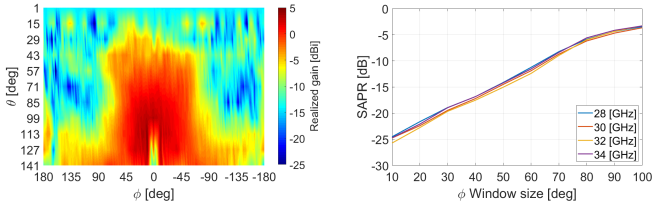


(a) (b)

Fig. 2. (a) Free space radiation pattern of the AUT, (b) SAPRs of four operating frequencies with the user in the same gesture.

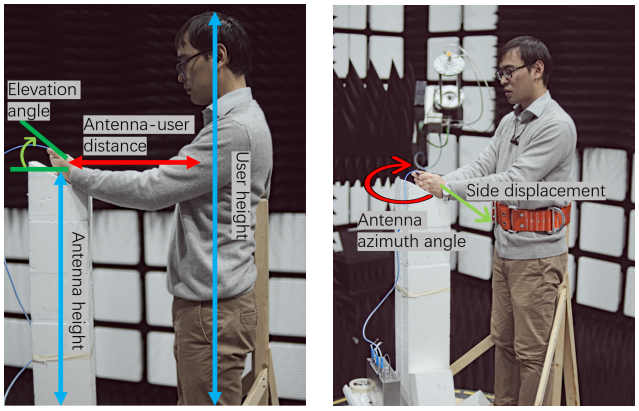


(a) (b)

Fig. 3. Setup of the user with a mobile phone at (a) data (single hand) mode, (b) dual hand mode.

As in optics, the user shadow size and strength are affected by the antenna-user related position. Five different sets of gestures in both data (single hand) and dual hand modes are concidured: the antenna-user height, the antenna-user distance, the antenna elevation angle, the antenna azimuth angle and the antenna side displacement are shown in Fig. 3. However, unlike the antenna-user height and the antenna-user distance, the shadow power is not sensitive to the antenna elevation angle, the antenna azimuth angle, and the antenna side displacement in both data and dual hand modes. Thus, in this section only the height and the distance assessments will be shown.

### *B. Antenna-user height*

First, measurements are conducted with the different relative antenna-user heights. The user's height is fixed as only a single person is participating in the measurement. The only variable is the AUT's height which is changed by adding different height styrofoam blocks on top of the column. The AUT is positioned at 100 cm, 115 cm and 130 cm above the platform which correspond to the user's waist, belly and chest height, respectively. In the paper these three heights are named as low, medium and high, respectively. The sampling resolution in $\theta$ and $\phi$ in this setup of 14° and 2° respectively are chosen to limit the measurement time to around 20 minutes. Shown in Fig. 4, as expected, the higher the AUT is placed the lower is the shadow appears in the plots, and the shadow widths are the same in all heights. The shadow above 0° in $\phi$ in the plot for the data mode and at both sides of the user in dual hand mode is due to the blockage of user's hand and arm.

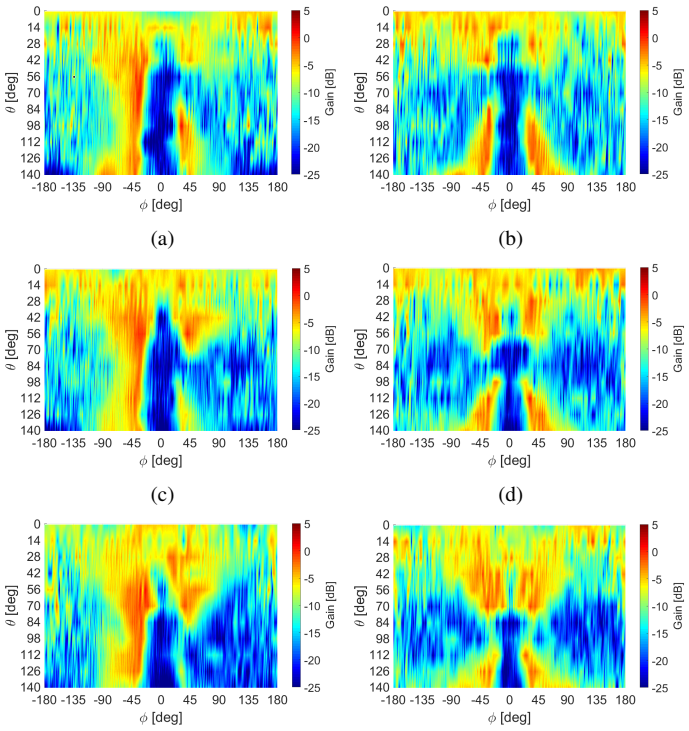


(a) (b) (c) (d) (e) (f)

Fig. 4. Radiation pattern with the user of (a) low AUT height for data mode, (b) low AUT height for dual hand mode, (c) medium AUT height for data mode, (d) medium AUT height for dual hand mode, (e) high AUT height for data mode, (f) high AUT height for dual hand mode.

The strongest shadow can be observed within $\phi = 0° \pm 15°$, and the whole body shadow is about 80° wide in $\phi$, which can be observed in Fig. 4. The $\phi$ window size is the window within $\pm\phi/2$. Then SAPRs and SCDFs are calculated based on these limits, and shown in Fig. 5. For the dual hand mode, it is clear that the SAPR increases with the height of the AUT for all $\phi$ window sizes in Fig. 5(b) and Fig. 5(d). The difference is around 3 dB within the small window sizes, and gets even smaller when the window size is close to the maximum shadow width 80°. For the small window sizes the main difference between the three patterns is the shadow height which mostly dictates the SAPR value. But as the window size increases, even more creeping wave and diffractions are accumulating in the shadowing region and thus the difference between the

curves is small. In data mode, the shadow height difference is not very clear for the low and medium AUT heights, as SAPRs for the two gestures are quite similar in Fig. 5(c). But for high height the shadow is obviously small. The SAPR snd SCDF figures show the same trend and difference as dual hand mode in Fig. 5(d) and Fig. 5(b). In most cases, the user shadow in dual hand mode is 1 to 2 dB smaller than that in data mode because of less blockage of hand and arm and more creeping wave in dual hand mode. Finally, it can be concluded that the user shadow is sensitive to the antenna-user height and it gets smaller as the AUT height increases.

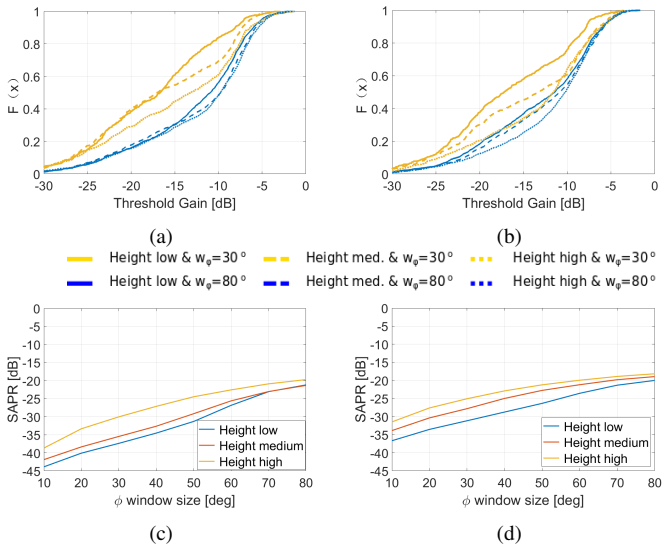


Fig. 5. SCDF comparison of different heights for (a) data mode, (b) dual hand mode, and SAPR comparison for (c) data mode, (d) dual hand mode.

### C. Antenna-user distance

The second critical gesture parameter is the antenna-user distance. In the original setups, the distance between the AUT and the user is 40 cm. Then, an extra styrofoam block is added between the user and the safety pole to decrease the distance to 30 cm. The antenna-user height is kept corresponding to the user's waist (low height). As both shadow height and width will be affected by the antenna-user distance, and the difference in distance is small in respect to the user's height, to see the more accurate difference in the radiation patterns, the sampling step in $\theta$ is set as 5° instead of 14°. To reduce the measurement time, the probe on the robot arm scans in $\theta$ while the platform turns with steps in $\phi$ in antenna-user distance investigation. And the step in $\phi$ is set as 5°, the test range is set as $-105°$ to 105° in $\phi$, and 5° to 130° in $\theta$ to keep the measurement time within 20 minites. As expected, shown in Fig. 6, the shadow width is larger when the distance is small for both data and dual hand modes. The same trend can be observed for the height of the shadow.

Finally, SCDFs and SAPRs are calculated for the two different antenna-user distances and shown in Fig. 7. It can be observed, that the SAPR for the setup with the distance of 40 cm is 2 to 3 dB higher than that for the distance of 30 cm for both data and dual hand modes. The SCDF distributions

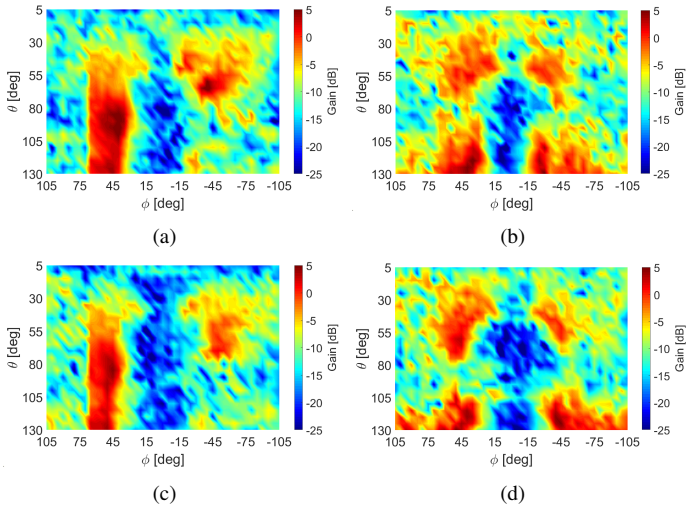


Fig. 6. Radiation pattern with the user of (a) 40 cm antenna-user distance for data mode, (b) 40 cm antenna-user distance for dual hand mode, (c) 30 cm antenna-user distance for data mode, (d) 30 cm antenna-user distance for dual hand mode.

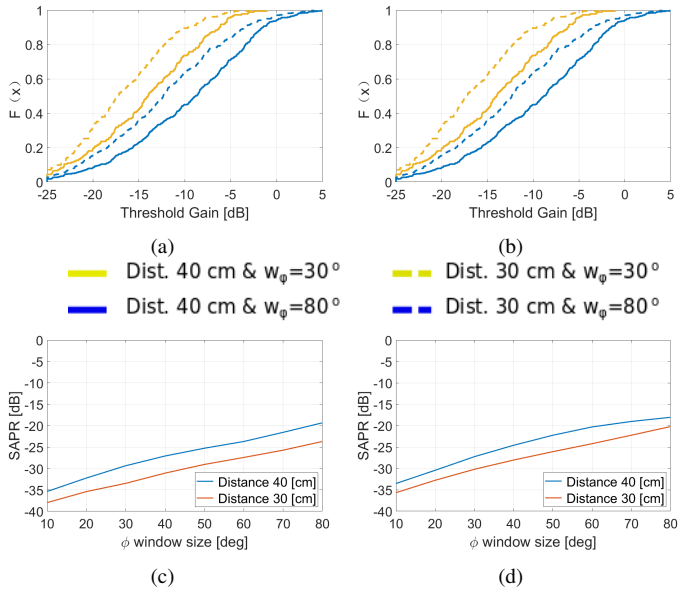


Fig. 7. SCDF comparison of different heights for (a) data mode, (b) dual hand mode, and SAPR comparison for (c) data mode, (d) dual hand mode.

agree well with the SAPR results and show the similar trend. Similarly to the measurements for the height investigation, the user shadow loss in the dual-hand mode is smaller than that in data mode. It can be concluded that the user shadow is sensitive to antenna-user distance and it gets smaller as the distance increases.

In this section it has been shown that two critical gestures are the relative antenna-user height and the antenna-user distance. Thus, when conducting a measurement campaign with the multiple users, these two variables will be taken into consideration.

## III. User Shadowed Intensity Ratio

Besides antenna-user positions, antenna gain and beam width may also affect the shadow pattern. While it is certain

that high gain can decrease the user shadow loss, to further investigate whether the user shadow shape and loss depends on the antenna beam width, three different horizontally polarized endfire antennas are measured. Sketched radiation patterns of the antennas are shown in Fig. 8. The antennas used for the measurements are the center element in arrays. The AUT 1 is the same one from the former measurements, the AUT 2 is the one proposed in [21] and has the widest beamwidth of the three, and the AUT 3 is the antenna used in [18] has the narrowest beamwidth. In the measurements, exactly the same positions of AUTs and user gestures are applied to minimize measurement error. Antenna efficiency and miss-match losses are calibrated out. Free space radiation patterns are shown in Fig. 9, and the beam width difference is obvious.

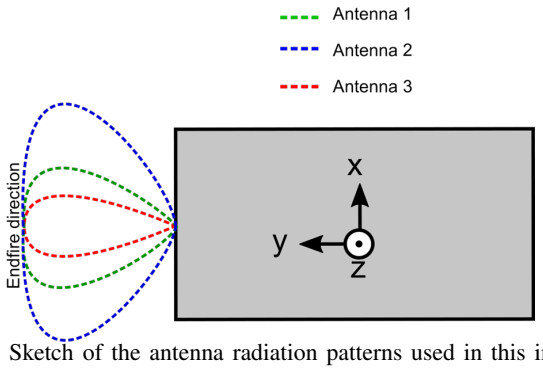


Fig. 8. Sketch of the antenna radiation patterns used in this investigation.

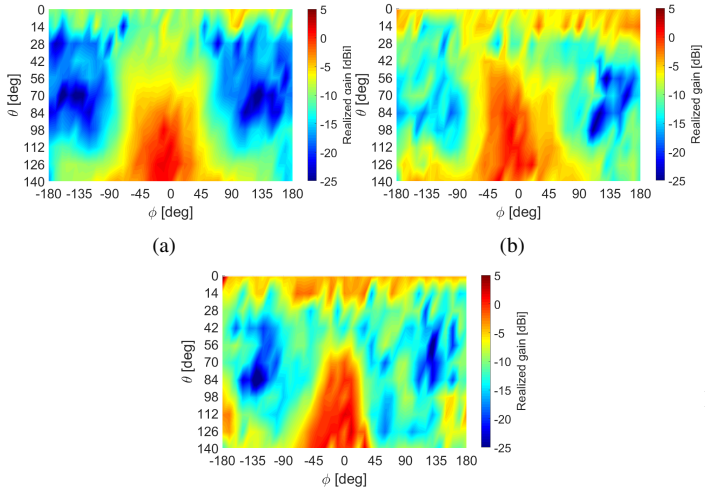


Fig. 9. Free space radiation pattern of (a) AUT 1, (b) AUT 2 and (c) AUT 3.

Then, the antennas are measured in both data and dual hand modes with the antenna height of 115 cm and antenna-user distance of 40 cm. Radiation patterns of three antennas in data mode are shown in Fig. 10. As expected, the widths and heights of the user's shadows are similar, but diffraction around the shadows differs as the illumination region depends on the beamwidth of the antennas. Next, to calibrate out the antennna gain difference and investigate the real shadowed intensity, the user shadowed intensity ratio (USIR) is used which is extracted from the free space radiation patterns and the radiation patterns with the user by the method defined in Equation. 3.

$$USIR(\theta,\phi) = 10 \cdot \log 10(G_{free}(\theta,\phi)/G_{user}(\theta,\phi)) \quad (3)$$

The values of $G_{user}$ and $G_{free}$ are the measured gain with and without the user for the AUT in exactly the same position and orientation. Processed data is shown in Fig. 11. The bigger the value of the USIR the stronger is the shadow. It can be noticed, that the shadow from the head is less severe for the AUT 3 which has the highest realized gain. However visually all three *USIRs* look similar. Then, SCDFs of the *USIRs* are plotted in Fig. 12. For the window sizes of 30° and 80° in both data and dual hand modes the observed difference is less than 2 dB which is not so significant and can be comparable to the measurement uncertainty of the chamber, equipment and user gesture.

It can be concluded that the *USIR* is not too sensitive to the AUT beam width and the antenna type. The de-embedding can be done for different types of the antenna with the accuracy of up to 2 dB. The shown de-embedding procedure will be used in statistical measurements in order to extract the *USIRs* for the multiple users and to make the model.

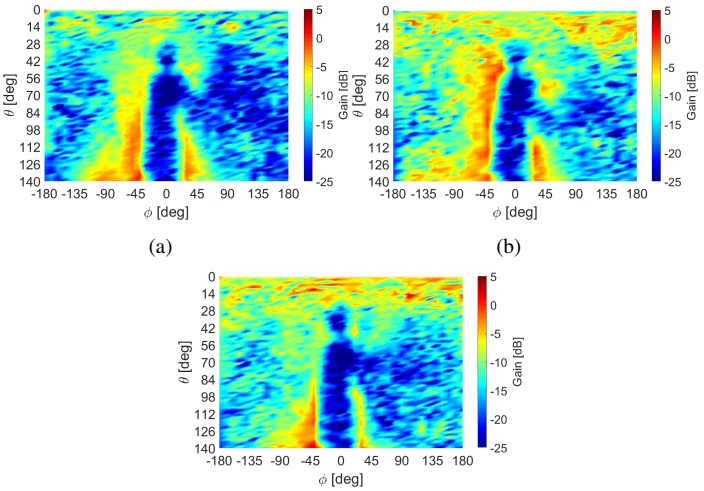


Fig. 10. Radiation pattern with the user of (a) AUT 1, (b) AUT 2 and (c) AUT 3 for data mode.

## IV. Statistical Measurement

In this section, multiple measurements with different subjects will be performed. Already in the Section II it has been found that both SAPR and SCDF depends mostly on the antenna-user height and also the distance between the person and the mobile device. Thus, here it has been chosen to use the two gestures with different the antenna-user height. As shown in Fig. 13, both data and dual hand mode measurements will be performed. The first AUT position is to user's waist in Fig. 13(a) representing the most common gesture when a user is operating the mobile device to access the social networks, watch videos or write text messages (in the case of dual-hand

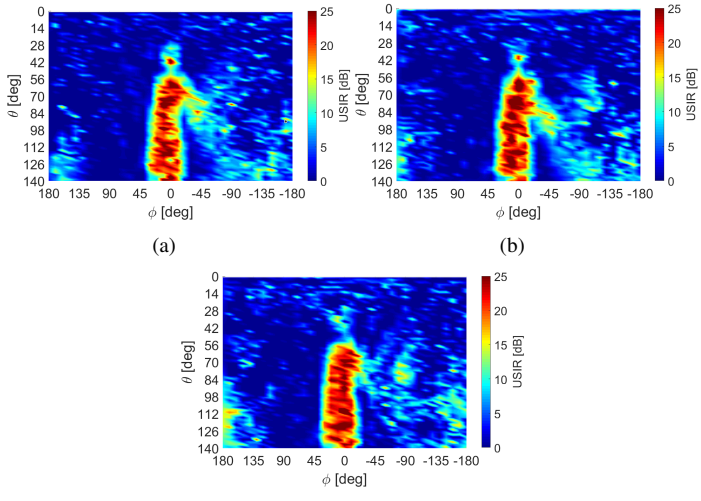


Fig. 11. USIR of (a) AUT 1, (b) AUT 2 and (c) AUT 3 for data mode.

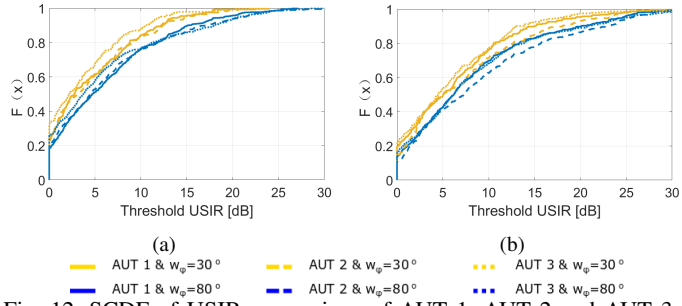


Fig. 12. SCDF of USIR comparison of AUT 1, AUT 2 and AUT 3 for (a) data mode, (b) dual hand mode.

mode in Fig. 13(c)). The second chosen gesture is at height of the user's chest in Fig. 13(b) and Fig. 13(d) and usually applied when user is operating the mobile device in order to take photos or make video calls. Furthermore, the gestures are chosen such so the user is holding the AUT comfortably, which means that the AUT height and distance between the user and AUT will be adjusted accordingly to the user's height and most comfortable grip position.

(a) (b) (c) (d)

Fig. 13. Gestures used in the statistical measurement: (a) data mode low position, (b) data mode high position, (c) dual hand mode low position, (d) dual hand mode high position.

### A. Sample Analysis

To find the right user sample for the measurement it is important to quantify the difference between male and female subjects in terms of radiation pattern, SAPR and SCDF. As it has been already shown in [12], the height of the user does play a significant role on the SAPR. However, until now, only male subjects have been measured for the frequencies around 28 GHz. First, to compare the user effect of the male to female subjects the radiation patterns are measured for two subjects with the same chosen height of 174 cm. The measurements have been done both in data and dual hand modes for all four gestures shown in Fig. 13. Next, four extra radiation patterns have been generated by mirroring the patterns around $\phi = 0°$ to take into account left and right-handed users and also to compensate for the non-symmetrical grip uncertainties in dual hand mode. In dual hand mode, the gesture will never be exactly symmetrical around the center of the mobile device as the most comfortable grip for the most subjects will never be exactly symmetrical.

Then, the mean *USP* have been computed for male and female subject with a height of 174 cm and shown in Fig. 14(a) and 14(b). The mean radiation patterns of different gender are visually quite similar, besides it can be noticed that the radiation pattern for the female subject does indeed have a triangle shaped shadowing under shoulder area because a a female torso is substantially different to that of a male one. But in mean radiation patterns of all male and female subjects as shown in Fig. 14(c) and 14(d), although the mean shadow of female is shorter than that of male as an average women have lower height than an avarage man, the shape difference is small.

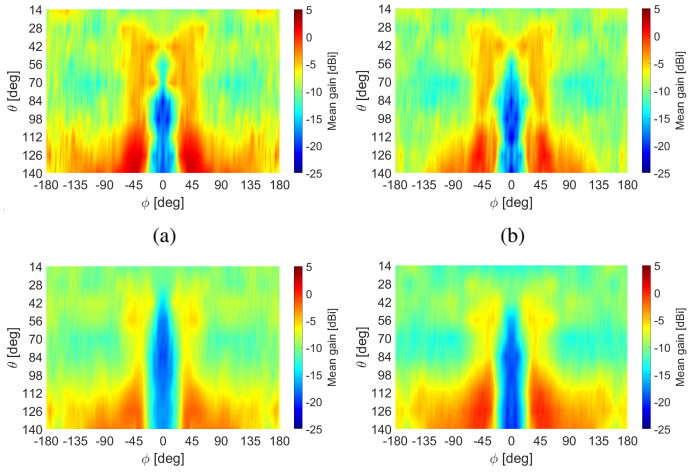


Fig. 14. Mean radiation pattern of (a) male and (b) female subject with a height of 174 cm, (c) all male and (d) all female subjects.

Also, in the SAPRs and SCDFs calculated from the two mean radiation patterns of subjects with the same height, the curves for the male and female subjects are very similar as shown in Fig. 15. Thus, it has been chosen to mix the male and female subjects together in one measurement campaign to reduce the total number of subjects.

The CDF distributions of men and women heights are shown in Fig. 16(a), which are based on measurement done in [22]. Total number of subject is 18, as described in [23] it is enought to provide statistical data on variation and the

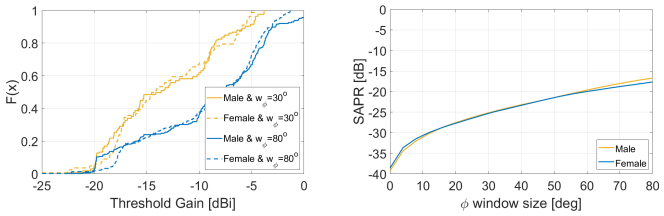


(a) (b)

Fig. 15. Comparison of (a) SCDF and (b) SAPR for the male and female subjects.

mean of the body loss. It can clearly be seen that men and women have very different mean heights, but the shape of the distribution is similar (The PDF will look like Gaussian bell curve). Thus when the two Gaussian distributions are put together the obtained new distribution will also be Gaussian. Furthermore, the population of men below 155cm and women above 175cm is limited and the performance will be special case. The scope of this study is focused on average adults. Hence, the men and women are combined together as samples and the resulting height PDF is shown in Fig. 16(b), which is approximately Gaussian with the mean of 175 cm. The more detailed description of the sample can be seen in Table I.

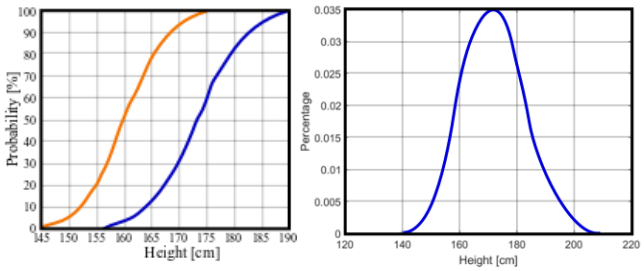


(a) (b)

Fig. 16. (a) CDF functions of the male and female height, (b) distribution of the sample height.

Table I. Number of chosen subjects for each corresponding height range.

| Height [cm] | <155 | 155-162 | 162-170 | 170-175 | 175-180 | 180-188 | > 188 |
|---|---|---|---|---|---|---|---|
| # of subjects | 1 | 2 | 5 | 2 | 5 | 2 | 1 |

### B. Measurement Results

The measurements have been performed from 1° to 140° in $\theta$ and -180° to 180° in $\phi$. In all of the measurements only one antenna has been used, which is the same one as in Section II. Only a single frequency of 28 GHz has been considered, as it has been already shown that in order to see any frequency dependency, the frequency range of at least 15 GHz should be chosen [23], but a mobile 5G antenna with such bandwidth is difficult to realize. However, because in measurements the antennas are pointing towards the user and the user hold angles are from 30° to 60°, the power collected by the probe at the $\theta \leq 42°$ is very low compared with the rest of the measured power. It has been chosen to cut this region in order to speed up the measurement time. Short measurement time facilitates decreasing the probability of the error due to user involuntary movements.

The mean radiation patterns are calculated for the data and dual hand modes from both gestures for all measurements with 18 people and shown in Fig. 17. Furthermore as in Fig. 14 extra radiation patterns are added to the mean by mirroring the existing measured radiation patterns around $\phi = 0°$ which makes the mean radiation pattern exactly symmetrical (accounting for the right and left-handed users). The mean radiation patterns for the data and dual hand mode look very similar, but a little bit more shadow from the hands can be observed in dual hand mode. This is expected because the user holds the mock-up more tight in dual hand mode than in data mode, also hand and arm blockage in data mode is reduced by mirroring.

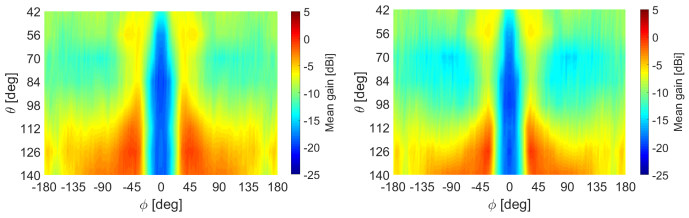


(a) (b)

Fig. 17. Measured mean radiation pattern calculated from 18 subjects for (a) data mode and (b) dual hand mode.

Nonetheless, the user shadow cannot be assessed properly if the radiation pattern is presented in the way in Fig. 17. In order to see the true user shadowed intensity, the antenna pattern needs to be de-embedded from the total radiation pattern based on the method shown in Section III. Even if multiple users have been measured it is possible to de-embedded the *USIRs* using two radiation patterns with different pointing angle of antenna in the free space. This can be done because users usually hold the mobile device in a very similar way in respect to each other [24]. One free space radiation pattern has been used for each of the gestures( high and low in Fig. 13) as shown in Fig. 18(a) for the top gesture (elevation angle of 60°) and the bottom gesture (elevation angle of 30°) in Fig. 18(b). it can clearly be noticed that the radiation patterns are very similar, because of the very wide beamwidth of the antenna [25]. The only significant difference between figures is the beam height, which also accours while the user is applying different heights gestures.

The *USIRs* for the data and dual hand modes are shown in Fig. 18(c) and Fig. 18(d) respectively. No significant difference can be observed between the two. Again, the shadow from the hands in dual hand mode is about 2 dB higher than that in data mode visually. In order to assess further the difference between the two modes both SAPR and SCDF is computed. The SCDF computed for the window sizes of 30° and 80 ° is shown for data and dual hand modes in Fig. 19(a). It can clearly be seen that the distribution of the USIR is similar for the data and dual hand modes. It can be concluded that all results from all measurements could be put together in order to make a more robust model of the *USIR* from the bigger sample size.

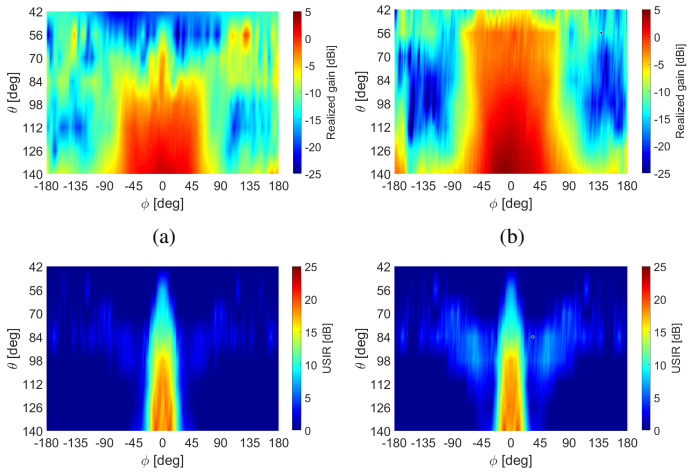


Fig. 18. (a) Free space radiation pattern in high position, (b) free space radiation pattern in low position, mean plot of (c) USIR for data mode, (d) USIR for dual hand mode.

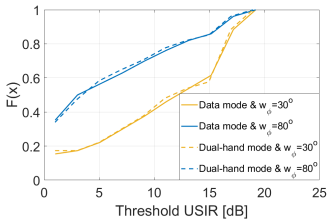


(a)

Fig. 19. SCDF of the data and dual hand modes.

## V. User Shadowed Pattern Modeling

In this section the model of the *USIR* will be presented. The proposed model is based on the statistical measurements with the multiple users, which have been presented in Section IV. The proposed model will be compared with the measured results by using metrics of mean *USIR* and SCDF.

As discussed earlier, it has been decided to combine the results from the data and dual hand modes as they has been shown to be similar in Section IV. This is done in order to obtain more data points and make a base for the model more robust. First, the mean *USIR* is calculated from all the available measurements is shown in Fig. 20(a). It can be noticed that this *USIR* looks quite similar to the *USIR* for data or dual hand modes in Fig. 18(c) or Fig. 18(d). The approximate size of the user blockage is 45° to -45° in $\phi$, while outside this range the shadow is very small.

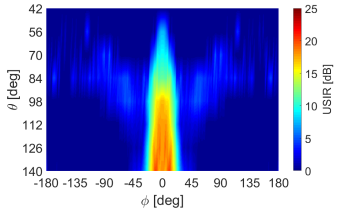


(a)

Fig. 20. Combined USIR result of the data and dual hand mode.

### A. USIR Modeling Procedure

In this paper, it has been chosen to model the *USIR* as a random process. However, visually it is clear that the distribution in the deep body shadow $\phi = \pm 15°$ is different than the distribution in the transitional regions (from shadow to non-shadow) at approximately 45° to 15° and -15° to -45° in $\phi$. However, it is not so straight forward to define those regions. This is why it has been chosen to take a look at SAPR calculated in $\phi$ and $\theta$ directions. First, SAPR is calculated for the variable window size from 6° to 80° in $\phi$, where the size of $\theta$ window is all the way from 42° to 140°. SAPR calculated in $\phi$ direction is shown in Fig. 21(a) and it can be noticed that two tendencies for all of the curves can be observed. From 6° to approximately 32° the curve increases steeply, however after 32° all three curves level. Thus, it has been chosen to use two regions for the model: one region of $\Delta\phi = \pm 16°$ and one where $\Delta\phi = \pm 16°$ to $\pm 45°$. Furthermore, SAPR calculated in $\theta$ direction is shown in Fig. 21(b). Here SAPR is calculated differently than in Fig. 21(a). Now it has been chosen to use sliding window of 14 ° and then calculate SAPR to each position of the window within $\Delta\phi = \pm 16°$. Here is quite difficult to identify different regions, such as head, shoulder and body regions. However, three tendencies for the mean curve can be observed. From 42° to 56° the curve increases steeply as the shadow presents. From 56° to 98° the curve is less steep while it can be defined as transitional region where diffracions, creeping wave and surface wave from the head occurs together with differernt user's height effect. However, after 98° the curve levels while it is the main body shadow region. Finally, all four regions are shown graphically in Fig. 21(c), where the region 1 is the region of the body shadow and regions 2, 3 and 4 are the transitional regions of body edge and head, respectively.

Furthermore, the plot of the variance for each spatial point on the 3D plot is shown in Fig. 21(d). It can be seen big variance appears within $\phi = \pm 16°$ which is the body shadow region. The other two big variance presents at $\theta = 140°$ $\phi = \pm 16°$. This phenomenon occurs due to the diffrations and creeping wave only presents at the body edge of the opposite side of the used hand in data mode while at both sides in dual hand mode. However this phenomenon does not result in big shadow in mean USIR, then it is going to be neglected in the modeling procedure.

As it has been discussed earlier, the regions in the *USIR* are based on the mean shadowed pattern from the measurements in both data and dual hand modes. However in order to model the *USIR* as a random process, the USIR in each spatial point within the region should follow a specific distribution. Nonetheless, regions 2 and 3 have similar distributions and only SCDFs for the regions 1,2 and 4 are shown in Fig. 22. Here, in order to make the model more simple, it has been chosen to fit the Gaussian distribution to the empirical curves which is defined as:

$$F(x) = \frac{1}{2}\left[1 + \mathrm{erf}\left(\frac{x-\mu}{\sigma\sqrt{(2)}}\right)\right] \tag{4}$$

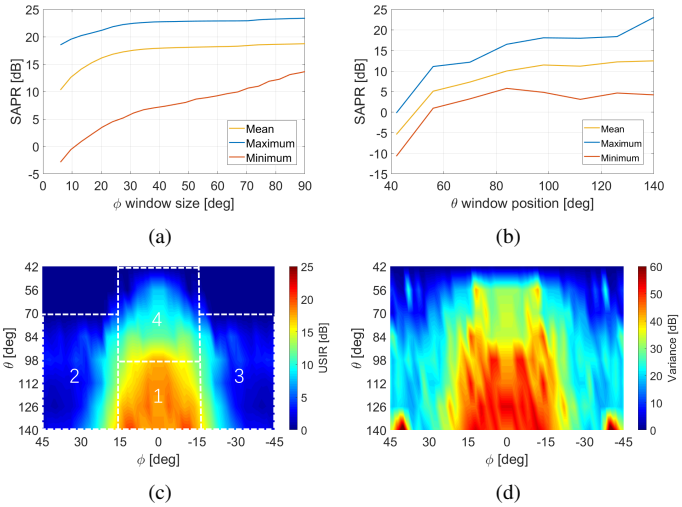


Fig. 21. (a) SAPR calculated in the phi window, (b) SAPR calculated in the theta window, and (c) regions defined to use in the model for USIR, (d) variance of USIR.

The standard deviation, mean and size of the three regions in Fig. 21(c) are given as:

1) region 1: $\mu = 16\,\text{dB}$ and $\sigma = 6\,\text{dB}$ ; size of the region: $\theta = 98°$ to $140°$, $\phi = \pm 16°$. All values are sorted based on big shadow intensities lie on the cener bottom of the plot. Values are sorted in $\theta$ direction as the highest values are at the bottom of the plot and the lowest ones are on the top. The values in $\phi$ plane are sorted so the highest values are in the middle of the plot $\phi = 0°$ and lowest values are at the edges $\phi = \pm 16°$.
2) region 2: $\mu = 2\,\text{dB}$ and $\sigma = 7\,\text{dB}$ ; size of the region: $\theta = 70°$ to $140°$, $\phi = 45°$ to $16°$. With the same basis in region 1, the values are sorted in $\phi$ plane so the highest values are closer to the middle of the plot $\phi = 16°$ and the lowest ones are at the edges $\phi = 45°$ .
3) region 3: $\mu = 2\,\text{dB}$ and $\sigma = 7\,\text{dB}$ ; size of the region: $\theta = 70°$ to $140°$, $\phi = -45°$ to $-16°$. Symmetrical to region 2, the values are sorted in $\phi$ plane so the highest values are closer to the middle of the plot $\phi = -16°$ and the lowest ones are at the edges $\phi = -45°$ .
4) region 4: $\mu = 3\,\text{dB}$ and $\sigma = 9\,\text{dB}$ ; size of the region: $\theta = 42°$ to $98°$, $\phi = \pm 16°$. All values are sorted based on big shadow intensities lie on the cener bottom of the plot. Values are sorted in $\theta$ direction as the highest values are at the bottom of the plot and the lowest ones are on the top. The values in $\phi$ plane are sorted so the highest values are in the middle of the plot $\phi = 0°$ and lowest values are at the edges $\phi = \pm 16°$.

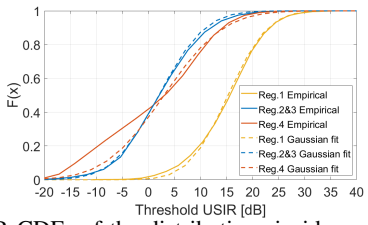


Fig. 22. USIR CDFs of the distributions inside region 1, 2 and 4.

In Fig. 22, Empirical curves are SCDF of all USIR of 18 users with four gestures and their mirrors. Gaussian fit curves are plots of the proposed distribution. It can be clearly noticed that the Gaussian curves fit the empirical ones very well. In region one, most of spatical points are above 0dB which agrrees with the main body shadow region. While due to the diffraction, creeping wave in region 2 and 3, about 38 percents of the total points in region 2 and 3 is below 0dB. For region 4, the Gaussian curve fits the empirial one quite well above 0dB, but not good with below. As in this region,it is not only includes the diffrations and creeping wave as region 2 and 3, difference of user's height also affects the result. As the main point of this paper is to investigate the user's shadow, then Gaussian fit of region 4 is prfered to fit the distribution above 0dB threshold USIR.

### *B. Model Accuracy Verification*

Then, in order to check if the proposed model is similar to the mean measured model it has been chosen to make a model in the Matlab and run the random process 36 times (corresponds to 18 data mode and 18 dual hand mode measurements) according to four regions Gaussian fit and sorting method mentioned above, which will yield in the 36 different *USIRs*. Furthermore, it has been chosen to also try to run the simulation for 360 times to see if there is a significant difference between the two calculated mean *USIRs*. The mean *USIRs* corresponding to the 36 and 360 process realizations are shown in Fig. 23(a) and 23(b). It can be seen that the *USIRs* in two cases look very similar and the shape agrees with the one in Fig. 21(c). However, the modeled figure is more clean as it can be explained from the fact that random processed result is sorted while sample chosen from the measurement is not perfect and has randomness. The SCDFs of empirical results and model are shown in Fig. 23(c) with $\phi$ window size of 30° and 80°. The distributions are very simular.

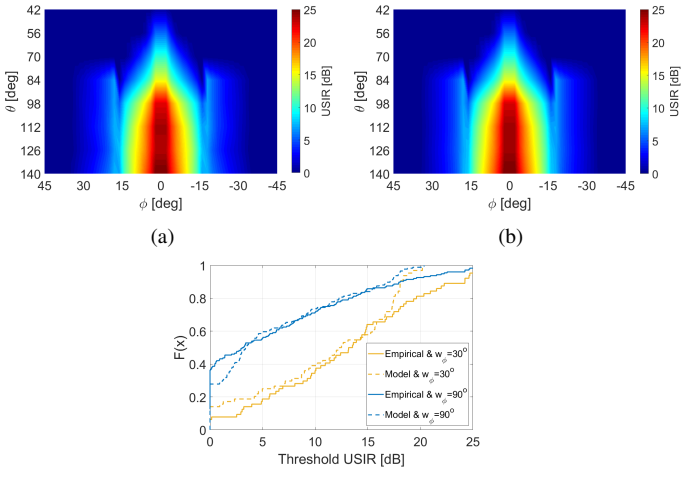


Fig. 23. (a) Mean USIR calculated from the 36 realizations of the random process, (b) mean USIR calculated from the 360 realizations of the random process, (c) USIR CDF of empirical and 36 times random process model.

Finally, the proposed model is compared with the 3GPP self-blocking model in portrait mode [15] as shown in Fig 24(a)

and Fig. 24(b). The proposed model gives a more realistic shape and distribution in the shadow region.

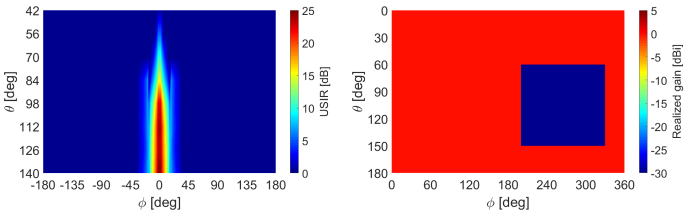


(a) (b)

Fig. 24. (a)USIR for the mean model made from 36 simulated realizations of the random process, (b)the 3GPP self blocking model in portrait mode.

Here it is clear that a reliable model of the *USIR* is proposed, the model accuracy is based on the sample chosen for the statistical measurement in Section IV.

## VI. Conclusion

In this work it has been shown that a reliable stochastic user shadow model can be constructed based on the measurement with multiple users and different gestures. The model is valid for the frequencies from 28 GHz to 34 GHz. The user shadow model is based on the measurement with 18 subjects of different heights and gender. However, it has been shown that difference between male and female subjects is not significant. The user shadow pattern is modeled as a random Gaussian process within the chosen spatial regions based on the mean user shadowed pattern obtained from the measurements. Furthermore, the measured users applied the gestures which ensured the highest variation in the user blockage. The measured mean user shadowed pattern has been de-embedded from the free radiation pattern of antenna and used as a base for the model. It has been shown that USIR can be done with accuracy of 2 dB and do not depend on the antenna type with the same polarization. To characterize the user shadow pattern, two metrics have been used: shadowing CDF and SAPR, where SAPR is calculated both along $\phi$ and $\theta$ directions. Finally, it has been shown that the proposed model have similar *USIR* and to the measured radiation pattern and gives a more realistic shape and ditribution in the shadow region than the 3GPP self-blocking model.

## References


[1] T. S. Rappaport, S. Sun, R. Mayzus, H. Zhao, Y. Azar, K. Wang, G. N. Wong, J. K. Schulz, M. Samimi, and F. Gutierrez, "Millimeter wave mobile communications for 5G cellular: It will work!," *IEEE Access*, vol. 1, pp. 335–349, 2013.

[2] J. Lee, E. Tejedor, K. Ranta-aho, H. Wang, K. T. Lee, E. Semaan, E. Mohyeldin, J. Song, C. Bergljung, and S. Jung, "Spectrum for 5G: Global status, challenges, and enabling technologies," *IEEE Comm. Mag.*, vol. 56, pp. 12–18, Mar. 2018.

[3] W. Roh, J. Y. Seol, J. Park, B. Lee, J. Lee, Y. Kim, J. Cho, K. Cheun, and F. Aryanfar, "Millimeter-wave beamforming as an enabling technology for 5G cellular communications: theoretical feasibility and prototype results," *IEEE Commun. Mag.*, vol. 52, pp. 106–113, February 2014.

[4] M. U. Rehman, X. Chen, C. G. Parini, and Z. Ying, "Evaluation of a statistical model for the characterization of multipath affecting mobile terminal GPS antennas in sub-urban areas," *IEEE Trans. Antennas Propag.*, vol. 60, pp. 1084–1094, Feb. 2012.

[5] J. Helander, K. Zhao, Z. Ying, and D. Sjöberg, "Performance analysis of millimeter-wave phased array antennas in cellular handsets," *IEEE Antenna Wireless Propag. Lett.*, vol. 15, pp. 504–507, 2016.

[6] T. Kang, S. Kim, K. I. Oh, J. H. Hwang, J. Lee, H. Park, K. Byun, and W. Lee, "Evaluation of human body characteristics for electric signal transmission based on measured body impulse response," *IEEE Transactions on Instrumentation and Measurement*, vol. 69, no. 9, pp. 6399–6411, 2020.

[7] Q. Tian, K. I. Wang, and Z. Salcic, "Human body shadowing effect on uwb-based ranging system for pedestrian tracking," *IEEE Transactions on Instrumentation and Measurement*, vol. 68, no. 10, pp. 4028–4037, 2019.

[8] A. Bernieri, G. Betta, D. Capriglione, G. Cerro, G. Miele, and M. S. D'Amata, "Lte human exposure evaluation: Maximum rf field strength extrapolation technique repeatability analysis," *IEEE Transactions on Instrumentation and Measurement*, pp. 1–1, 2020.

[9] J. Krogerus, J. Toivanen, C. Icheln, and P. Vainikainen, "Effect of the human body on total radiated power and the 3-d radiation pattern of mobile handsets," *IEEE Transactions on Instrumentation and Measurement*, vol. 56, no. 6, pp. 2375–2385, 2007.

[10] E. Conil, A. Hadjem, A. Gati, M. Wong, and J. Wiart, "Influence of plane-wave incidence angle on whole body and local exposure at 2100 mhz," *IEEE Transactions on Electromagnetic Compatibility*, vol. 53, no. 1, pp. 48–52, 2011.

[11] J. B. Andersen, J. O. Nielsen, and G. F. Pedersen, "Absorption related to hand-held devices in data mode," *IEEE Transactions on Electromagnetic Compatibility*, vol. 58, no. 1, pp. 47–53, 2016.

[12] I. Syrytsin, S. Zhang, G. F. Pedersen, K. Zhao, T. Bolin, and Z. Ying, "Statistical investigation of the user effects on mobile terminal antennas for 5G applications," *IEEE Trans. Antennas Propag.*, vol. 65, pp. 6596–6605, Dec 2017.

[13] K. Zhao, J. Helander, D. Sjöberg, S. He, T. Bolin, and Z. Ying, "User body effect on phased array in user equipment for the 5G mmwave communication system," *IEEE Antenna Wireless Propag. Lett.*, vol. 16, pp. 1847–1850, 2017.

[14] T. Wang, M. Umehira, H. Otsu, S. Takeda, T. Miyajima, and K. Kagoshima, "A twin cylinder model for moving human body shadowing in 60GHz wlan," in *2015 21st Asia-Pacific Conference on Communications (APCC)*, pp. 188–192, Oct 2015.

[15] 3GPP, "Technical specification group radio access network; study on channel model for frequencies from 0.5 to 100 ghz," *document TR 38.901*, Jul. 2017.

[16] B. Yu, K. Yang, C. Y. D. Sim, and G. Yang, "A novel 28 GHz beam steering array for 5G mobile device with metallic casing application," *IEEE Trans. Antennas Propag.*, vol. 66, pp. 462–466, Jan. 2018.

[17] R. Rodriguez-Cano, S. Zhang, K. Zhao, and G. F. Pedersen, "Reduction of main beam-blockage in an integrated 5g array with a metal-frame antenna," *IEEE Transactions on Antennas and Propagation*, vol. 67, pp. 3161–3170, May 2019.

[18] I. Syrytsin, S. Zhang, and G. F. Pedersen, "User impact on phased and switch diversity arrays in 5G mobile terminals," *IEEE Access*, vol. 6, pp. 1616–1623, 2018.

[19] I. Syrytsin, S. Zhang, G. F. Pedersen, and A. S. Morris, "User-shadowing suppression for 5g mm-wave mobile terminal antennas," *IEEE Transactions on Antennas and Propagation*, vol. 67, pp. 4162–4172, June 2019.

[20] V. Raghavan, L. Akhoondzadeh-Asl, V. Podshivalov, J. Hulten, M. A. Tassoudji, O. H. Koymen, A. Sampath, and J. Li, "Statistical blockage modeling and robustness of beamforming in millimeter-wave systems," *IEEE Transactions on Microwave Theory and Techniques*, pp. 1–15, 2019.

[21] M. M. Samadi Taheri, A. Abdipour, S. Zhang, and G. F. Pedersen, "Integrated millimeter-wave wideband end-fire 5g beam steerable array and low-frequency 4g lte antenna in mobile terminals," *IEEE Transactions on Vehicular Technology*, vol. 68, pp. 4042–4046, April 2019.

[22] J. Panero and M. Zelnik, *Human Dimension and Interior Space: A Source Book of Design Reference Standards*. Watson-Guptill, 1979.

[23] J. O. Nielsen, G. F. Pedersen, K. Olesen, and I. Z. Kovacs, "Statistics of measured body loss for mobile phones," *IEEE Transactions on Antennas and Propagation*, vol. 49, no. 9, pp. 1351–1353, 2001.

[24] M. Pelosi, O. Franek, G. F. Pedersen, and M. Knudsen, "User's impact on pifa antennas in mobile phones," in *VTC Spring 2009 - IEEE 69th Vehicular Technology Conference*, pp. 1–5, April 2009.

[25] I. Syrytsin, S. Zhang, G. F. Pedersen, and A. Morris, "Compact quad-mode planar phased array with wideband for 5G mobile terminals," *IEEE Trans. Antennas Propag.*, 2018,(in press).

**Peiye Liu** was born in Harbin, China, in 1985. He received the M.S. degree in wireless and photonics engineering from Chalmers university of technology, Gothenburg, Sweden, in 2016. After M.S. studies, he joined Guangdong Shenglu telecommunication techonlogy, co., LTd. Currntly, he is a guest researcher at Department of Electronic System at Aalborg University. His research interests include planner array antennas, mm-wave mobile antenna design and interactions beteewn user and mobile antennas.

**Igor Syrytsin** was born in Saratov, Russia, in 1988. He received the B.S. degree in electronic engineering and IT and M.S. degree in wireless communication systems from Aalborg University, Aalborg, Denmark, in 2014 and 2016, respectively. Currently, he is pursuing the Ph.D. degree at Department of Electronic Systems at Aalborg University. His research interests include microwave, mm-wave mobile antenna and phased array design and interactions between user and mobile antennas.

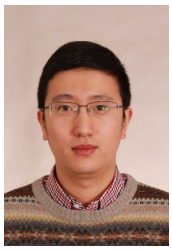

**Shaui Zhang** received the B.E. degree from the University of Electronic Science and Technology of China, Chengdu, China, in 2007 and the Ph.D. degree in electromagnetic engineering from the Royal Institute of Technology (KTH), Stockholm, Sweden, in 2013. After his Ph.D. studies, he was a Research Fellow at KTH. In April 2014, he joined Aalborg University, Denmark, where he currently works as Associate Professor. In 2010 and 2011, he was a Visiting Researcher at Lund University, Sweden and at Sony Mobile Communications AB, Sweden, respectively. He was also an external antenna specialist at Bang & Olufsen, Denmark from 2016-2017. He has coauthored over 40 articles in well-reputed international journals and over 14 (US or WO) patents. His research interests include: mobile terminal mm-wave antennas, biological effects, CubeSat antennas, UWB wind turbine blade deflection sensing, MIMO antenna systems, and RFID antennas.

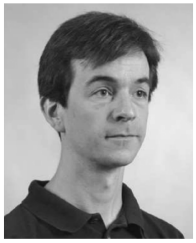

**Jesper Ødum Nielsen** received the master's degree in electronics engineering and the Ph.D. degree from Aalborg University, Aalborg, Denmark, in 1994 and 1997, respectively. He is currently at the Department of Electronic Systems, Antennas, Propagation and Millimeter-Wave Systems Section, Aalborg University. His current research interests include experimental investigation of the mobile radio channel and the influence mobile device users have on the channel. Among other things, he has been involved in massive MIMO and mm-wave channel sounding and modeling, and measurements using live GSM and LTE networks. In addition, he has been working with radio performance evaluation, including over the air testing of active wireless devices

**Gert Frølund Pedersen** was born in 1965. He received the B.Sc. and E.E. (Hons.) degrees in electrical engineering from the College of Technology in Dublin, Dublin Institute of Technology, Dublin, Ireland, in 1991, and the M.Sc.E.E. and Ph.D. degrees from Aalborg University, Aalborg, Denmark, in 1993 and 2003, respectively. Since 1993, he has been with Aalborg University where he is a Full Professor heading the Antenna, Propagation and Networking LAB with 36 researchers. He is also the Head of the Doctoral School on wireless communication with some 100 Ph.D. students enrolled. His research interests include radio communication for mobile terminals especially small antennas, diversity systems, propagation, and biological effects. He has published more than 175 peer reviewed papers and holds 28 patents. He has also worked as a Consultant for developments of more than 100 antennas for mobile terminals including the first internal antenna for mobile phones in 1994 with lowest SAR, first internal triple-band antenna in 1998 with low SAR and high TRP and TIS, and lately various multiantenna systems rated as the most efficient on the market. He has worked most of the time with joint university and industry projects and have received more than 12 M$ in direct research funding. He is currently the Project Leader of the SAFE project with a total budget of 8 M$ investigating tunable front end including tunable antennas for the future multiband mobile phones. He has been one of the pioneers in establishing over-the-air measurement systems. The measurement technique is now well established for mobile terminals with single antennas and he was chairing the various COST groups (swg2.2 of COST 259, 273, 2100, and now ICT1004) with liaison to 3GPP for over-the-air test of MIMO terminals. He is currently involved in MIMO OTA measurement.